# Joint Planning of Smart EV Charging Stations and DGs in Eco-friendly Remote Hybrid Microgrids

Mostafa F. Shaaban, *Member, IEEE,* Sayed Mohamed, Muhammad Ismail, *Senior Member, IEEE,* Khalid Qaraqe, *Senior Member, IEEE,* and Erchin Serpedin, *Fellow, IEEE*

***Abstract*—This paper proposes an efficient planning algorithm for allocating smart electric vehicle (EV) charging stations in remote communities. The planning problem jointly allocates and sizes a set of distributed generators (DGs) along with the EV charging stations to balance the supply with the total demand of regular loads and EV charging. The planning algorithm specifies optimal locations and sizes of the EV charging stations and DG units that minimize two conflicting objectives: (a) deployment and operation costs and (b) associated green house gas emissions, while satisfying the microgrid technical constraints. This is achieved by iteratively solving a multi-objective mixed integer non-linear program. An outer sub-problem determines the locations and sizes of the DG units and charging stations using a non-dominated sorting Genetic algorithm (NSGA-II). Given the allocation and sizing decisions, an inner sub-problem ensures smart, reliable, and eco-friendly operation of the microgrid by solving a non-linear scheduling problem. The proposed algorithm results in a Pareto frontier that captures the trade-off between the conflicting planning objectives. Simulation studies investigate the performance of the proposed planning algorithm in order to obtain a compromise planning solution.**

***Index Terms*—EV charging stations, remote microgrids, islanded microgrids, hybrid microgrids, microgrid planning.**

## I. Introduction

REMOTE communities are challenged by a limited access to fossil fuel. One effective approach to reduce the dependance on fossil fuel strives to rely more on electric vehicles (EVs). In addition, wide adoption of EVs promotes eco-friendliness in remote communities since EVs are characterized by zero green house gas (GHG) emissions. However, to ensure effective wide adoption of EVs, efficient planning algorithms are required to properly allocate and size EV charging stations in such remote microgrids.

Research works in literature focus mainly on smart operation strategies of EV charging stations [1] - [12]. In specific, temporal coordination of EV charging demands is adopted to satisfy the EV charging requests subject to the microgrid technical constraints. Limited attention is given in literature to planning problems of EV charging stations in the distribution grid [13] - [16]. A natural question that arises in this case is how to balance the supply with the total demand in terms of the regular loads and the EV charging. One way to handle this issue is to consider a microgrid setting with an already installed set of distributed generators (DGs) and rely on demand response strategies to balance the supply with the total demand while allocating the EV charging stations [17]. However, such an approach might lead to infeasible solutions for wide deployment of EV charging stations. Hence, the tolerance gained by adopting demand response strategies can lead to only a limited number of EV charging stations that can be installed in the microgrid while satisfying the power balance constraints. This limited number of installed EV stations might be insufficient to serve the expected EV charging requests. This challenge is more pronounced in a remote microgrid that operates in an islanded mode, and hence, isolated from the main bulk generation. Consequently, a more effective approach is to jointly allocate EV charging stations and DGs in order to balance both supply and demand while serving the EV charging requests and satisfying the grid technical constraints. Again, to reduce the dependance on fossil fuel and promote a sustainable and eco-friendly remote community, a mixed set of renewable and non-renewable DGs should be deployed. Unfortunately, the literature lacks an efficient planning algorithm that can jointly allocate and size both DGs and EV charging stations in a remote microgrid while satisfying the microgrid technical constraints and accounting for the intermittent nature of the renewable DGs and the coordinated nature of EV charging.

This paper fills the gap in literature by proposing an efficient joint planning algorithm for EV charging stations and DGs in remote microgrids. The main contributions of the proposed joint planning algorithm can be summarized as follows:

- The planning problem is formulated as a multi-objective mixed integer non-linear program (MINLP) that jointly specifies optimal locations and sizes of renewable and non-renewable mix of DG units and EV charging stations in remote islanded microgrids. The multi-objective function of the planning problem considers both economical and environmental dimensions in terms of capital and operation costs, CAPEX and OPEX, respectively, along with GHG emissions. Furthermore, the formulated problem accounts for the operational feasibility of the planning decisions in terms of active and reactive power balance, voltage and frequency stability, and reserve margin constraints. Moreover, appropriate stochastic modeling is considered in the problem formulation for the intermittent renewable DG units along with random arrivals and departures of EV charging requests.
- An efficient planning algorithm is proposed to solve the NP-hard joint planning problem. An outer sub-problem allocates and sizes the DGs and EV charging stations, and hence, specifies the CAPEX, following a non-dominated sorting Genetic algorithm (NSGA-II). On the other hand, an inner sub-problem ensures that the planning decisions

M. F. Shaaban is with the Department of Electrical and Computer Engineering, University of Waterloo, Waterloo, Canada, e-mail: m2farouk@uwaterloo.ca. S. Mohamed, M. Ismail, and K. Qaraqe are with the Department of Electrical and Computer Engineering, Texas A&M University at Qatar, Doha, Qatar, e-mail: {sayed.mohamed, m.ismail, khalid.qaraqe}@qatar.tamu.edu. E. Serpedin is with the Department of Electrical and Computer Engineering, Texas A&M University, College Station, TX, USA, email: eserpedin@tamu.edu.



https://doi.org/10.1109/TSG.2019.2891900

reached by the outer sub-problem satisfies the microgrid technical constraints and determines the expected OPEX and the associated GHG emissions. The two sub-problems are solved iteratively and an optimal Pareto frontier is obtained, which captures the trade-off between the conflicting objective functions.
- Simulation studies are carried out to investigate the performance of the planning algorithm. A compromise joint planning solution is shown to offer an acceptable performance for the conflicting objectives.

The rest of this paper is organized as follows. The system model is presented in Section II. The problem formulation and the proposed planning algorithm are given in Sections III and IV, respectively. Simulation results are discussed in Section V, and conclusions are outlined in Section VI.

## II. System Model

This section describes the system model in terms of the stochastic models, hybrid microgrid setting, dispatchable and renewable DG models, EV coordinated charging mechanism, and the charging price model, in addition to the GHG emission models.

### A. Stochastic Models

Define a set of scenarios $\mathcal{Y}$ that are used to capture the stochastic nature of the problem in terms of regular load consumptions, generation from the renewable-based DG units, and EV demands. Each scenario $y \in \mathcal{Y}$ is further divided into set of periods $\mathcal{T}$ with equal duration $\tau$.

In order to generate $\mathcal{Y}$, historical data are used for the regular load consumptions, solar irradiance, and EV arrivals and parking durations in a parking lot. The year is divided into 4 seasons, and each season is represented by two days, namely, weekday and weekend. The available data within each day type in each season is discretized using K-means clustering. Cumulative distributed functions (CDFs) are calculated for the regular load consumptions, solar irradiance, and EV arrivals and parking durations at each hour over each day type in each season. Furthermore, the desired EV battery state-of-charge (SOC) and the initial SOC are assumed to follow standard uniform distributions bounded by lower and upper values that are selected according to the available EVs in the market. Using the developed CDFs and random SOC models, scenario $y \in \mathcal{Y}$ can be generated with probability $p(y)$ to model a realization of the regular load consumptions, generation from the renewable-based DG units, and EV charging demands.

### B. Hybrid Microgrid Model

Consider a remote hybrid AC/DC islanded microgrid that consists of two disjoint sets of AC buses, $\mathcal{N}_{\text{AC}}$ and DC buses, $\mathcal{N}_{\text{DC}}$. The union of the disjoint subsets of AC and DC buses is denoted by $\mathcal{N}$. Let $\mathcal{K}$ represent a set of AC/DC interlinking converters that are located within the microgrid to transfer the power between the AC and DC sections of the microgrid.

Let $P_{k,n}(t,y)$ and $Q_{k,n}(t,y)$ denote the active and reactive powers at converter $k \in \mathcal{K}$ on bus $n \in \mathcal{N}$ at time instant $t \in \mathcal{T}$ for scenario $y \in \mathcal{Y}$, respectively. The maximum apparent power capability for converter $k \in \mathcal{K}$ is denoted by $S_{k,n}^{\max}$. For bus $n \in \mathcal{N}$, let $P_n(t,y)$ and $P_{\text{L},n}(t,y)$ denote the net injected active power and the load active consumption, respectively. On the other hand, the net injected reactive power and the load reactive consumption are defined only for bus $n \in \mathcal{N}_{\text{AC}}$ as $Q_n(t,y)$ and $Q_{\text{L},n}(t,y)$, respectively.

For bus $n \in \mathcal{N}$, the voltage magnitude and angle is given by $V_n(t,y)$ and $\delta_n(t,y)$, respectively. The upper and lower limits for the voltage magnitude $V_n(t,y)$ are denoted as $V^{\max}$ and $V^{\min}$, respectively. Similarly, the upper and lower limits for the system operation frequency $\omega(t,y)$ are $\omega^{\max}$ and $\omega^{\min}$, respectively. For two buses $n$ and $n' \in \mathcal{N}_{\text{AC}}$, define the magnitude and angle of the Y-bus element as $Y_{n,n'}$ and $\theta_{n,n'}$, respectively. Also, for two buses $n$ and $n' \in \mathcal{N}_{\text{DC}}$, let the $G_{n,n'}$ denote the conductance.

### C. DG Models

The set of available generation technologies is denoted as $\mathcal{D}$, which is further divided into two disjoint sub-sets, namely, $\mathcal{D}_1$ and $\mathcal{D}_2$ for dispatchable (gas-based) generators and renewable (PV-based) DGs, respectively. Binary decision variable $x_{d,n}$ defines whether DG technology $d \in \mathcal{D}$ is allocated on bus $n \in \mathcal{N}$ ($x_{d,n} = 1$) or not ($x_{d,n} = 0$). By default, a DG $d \in \mathcal{D}_1$ is allocated on a bus in $\mathcal{N}_{\text{AC}}$ while a DG $d \in \mathcal{D}_2$ is allocated on a bus in $\mathcal{N}_{\text{DC}}$. Such an approach is adopted in order to avoid the extra cost required for the installation of converters. For any DG unit $d \in \mathcal{D}$, let the capital cost and capital recovery factor be $C_{\text{C},d}$ and $R_d$, respectively. Denote the first year annual OPEX for DG $d \in \mathcal{D}$ by $C_{0,d}$ in \$, which accounts for the fuel cost for the dispatchable generators in $\mathcal{D}_1$. As a result, the levelized OPEX can be defined as $C_{\text{L},d} = C_{0,d} f_d R_d$ with $f_d$ represents the present value function [18]. The active power injected on bus $n \in \mathcal{N}$ by any DG unit $d \in \mathcal{D}$ is denoted by $P_{d,n}(t,y)$ and the DG unit total capacity is $P_{d,n}^{\max}$. The generated solar power from a PV unit $P_{\text{PV}}(t,y)$ is defined as a fraction of the PV unit total capacity.

Let $Q_{d,n}(t,y)$ denote the reactive power injected by DG unit $d \in \mathcal{D}_1$ on bus $n \in \mathcal{N}_{\text{AC}}$. The apparent capacity for $d \in \mathcal{D}_1$ is given by $S_{d,n}^{\max}$. Droop control is applied to stabilize the voltage and frequency levels within the microgrid. Define $\hat{\omega}_{d,n}(t,y)$ and $\hat{V}_{d,n}(t)$ as the no-load reference frequency and voltage settings for the DG unit $d$, respectively. Let $\alpha_{d,n}(t,y)$ and $\beta_{d,n}(t,y)$ denote the droop slope for active and reactive powers of the DG unit, respectively.

### D. EV Models

Let $\mathcal{M}$ denote a set of smart EV charging stations. The set of chargers available at a given charging station $m \in \mathcal{M}$ is given by $\mathcal{I}_m$, which has a minimum number of $I_m^{\min}$ and a maximum number of $I_m^{\max}$ chargers. Let $x_{m,n}$ represent a binary decision variable that indicates whether a charging station $m$ is allocated on bus $n \in \mathcal{N}_{\text{DC}}$ ($x_{m,n} = 1$) or not ($x_{m,n} = 0$). Also, let $x_{i_m,n}$ be a binary decision variable that indicate whether charger $i_m$ is allocated in charging station $m$ ($x_{i_m,n} = 1$) or not ($x_{i_m,n} = 0$). Define the CAPEX and

capital recovery factor per charger $i$ in station $m$ to be $C_{\mathrm{C},i}$ and $R_i$, respectively. The charger capacity is denoted as $P^{\max}_{i_m,n}$.

Let $z_{i_m,n}(t,y)$ denote a binary charging decision variable that indicates if an EV connected to charger $i_m \in \mathcal{I}_m$ in charging station $m \in \mathcal{M}$ should be charged during period $t \in \mathcal{T}$ for scenario $y \in \mathcal{Y}$ ($z_{i_m,n}(t,y)=1$) or not ($z_{i_m,n}(t,y)=0$). Denote $B^{\mathrm{INT}}_{i_m,n}(t,y)$, $B^{\mathrm{DES}}_{i_m,n}(t,y)$, and $B^{\mathrm{FN}}_{i_m,n}(t,y)$ as the initial, desirable, and final SOC values during period $t$ and scenario $y$ for an EV connected to charger $i_m$ in charging station $m$ that is allocated on bus $n$. The battery capacity for an EV that is connected to charger $i_m$ is given by $E^{\max}_{i_m,n}$ and the energy delivered to the EV's battery by the end of period $t$ is denoted as $E_{i_m,n}(t,y)$. The charger's power transfer limit is $P^{\mathrm{CH}}_{i_m,n}(t,y)$, the consumed power by an EV connected to charger $i_m$ in station $m$ allocated at bus $n$ is $P_{i_m,n}(t,y)$, and the charger's efficiency is $\eta$.

A linear price model is adopted to reflect the dependency between the charging price $\rho_{m,n}(t,y)$ in kWh and the amount of requested charging by the EV owner as described by the desirable SOC $B^{\mathrm{DES}}_{i_m,n}(t,y)$. Specifically, the charging price presents maximum and minimum values of $\rho^{\max}$ and $\rho^{\min}$, respectively. At a specific period $t$ and scenario $y$, when the charging price is set to $\rho^{\max}$, $B^{\mathrm{DES}}_{i_m,n}(t,y)$ is set to a minimum value $B^{\min}$. On the other hand, when the charging price is set to $\rho^{\min}$, $B^{\mathrm{DES}}_{i_m,n}(t,y)$ is set to a maximum value $B^{\max}$. In between, a linear relationship is assumed between the charging price and the desirable SOC, i.e., $B^{\mathrm{DES}}_{i_m,n}(t,y) = B^{\max} - \Delta\rho_{m,n}(t,y)$, where the slope $\Delta = (B^{\max}-B^{\min})/(\rho^{\max}-\rho^{\min})$.

### *E. Green House Gas Emission Models*

Two elements contribute to the amount of GHG emissions in the microgrid, namely, the dispatchable DG units and the EVs. Let $\mu_d$ denote the amount of emitted GHG in kg for each generated kWh of energy from dispatchable DG $d \in \mathcal{D}_1$. For conventional fossil-fueled vehicles, denote the amount of emitted GHG in kg for each driven km by $\nu$. When an EV replaces a conventional vehicle, the amount of emitted GHG will be reduced due to the zero emissions of EVs. To account for such a reduction, define $D$ as the distance traveled in km for each kWh charging of the EV.

## III. Problem Formulation

The formulation of the multi-objective planning problem in a remote hybrid micro-grid covers both economical and environmental aspects while satisfying the technical constraints. Both CAPEX and OPEX of different components are accounted for and various technical constraints are considered to ensure the feasibility of the proposed planning solution.

### *A. Economical Objective*

The first objective of the planning problem is to jointly allocate and size the DG units and EV charging stations in a manner that minimizes the annualized CAPEX and levelized OPEX over all possible scenarios. The total annualized costs can be expressed as

$$C_{\mathrm{T}} = C_{\mathrm{CT}} + C_{\mathrm{OT}}, \tag{1}$$

where $C_{\mathrm{CT}}$ denotes the total annualized CAPEX and $C_{\mathrm{OT}}$ represents the expected levelized OPEX.

The total annualized CAPEX accounts for the investments required to install the DG units and the EV charging stations, and hence, it can be expressed as

$$C_{\mathrm{CT}} = C_{\mathrm{CD}} + C_{\mathrm{CM}}, \tag{2}$$

where $C_{\mathrm{CD}}$ and $C_{\mathrm{CM}}$ represent the total annualized CAPEX for the DG units and the EV charging stations, respectively. For the DGs in $\mathcal{D}$, the total annualized CAPEX is given by

$$C_{\mathrm{CD}} = \sum_{n\in\mathcal{N}}\sum_{d\in\mathcal{D}} x_{d,n} P^{\max}_{d,n} C_{\mathrm{C},d} R_d. \tag{3}$$

Similarly, the annualized CAPEX of the EV stations is given by

$$C_{\mathrm{CM}} = \sum_{n\in\mathcal{N}_{\mathrm{DC}}}\sum_{m\in\mathcal{M}} x_{m,n} \sum_{i_m\in\mathcal{I}_m} x_{i_m,n} P^{\max}_{i_m,n} C_{\mathrm{C},i} R_i, \tag{4}$$

with $I^{\min}_m \le i_m \le I^{\max}_m$.

The expected levelized OPEX $C^{\mathrm{OP}}$ is described as the difference between the expected fuel cost of the dispatchable generators in $\mathcal{D}_1$ and the expected profit from the investment in the EV charging stations, i.e.,

$$C^{\mathrm{OP}} = C^{\mathrm{OP}}_{\mathrm{D}} - C^{\mathrm{OP}}_{\mathrm{M}}, \tag{5}$$

where the levelized expected OPEX due to the DG units, $C^{\mathrm{OP}}_{\mathrm{D}}$, is given by

$$C^{\mathrm{OP}}_{\mathrm{D}} = \sum_{y\in\mathcal{Y}} p(y) \sum_{t\in\mathcal{T}}\sum_{n\in\mathcal{N}_{\mathrm{AC}}}\sum_{d\in\mathcal{D}_1} x_{d,n} C_{\mathrm{L},d} P_{d,n}(t,y), \tag{6}$$

and the expected profit due to the EV charging station, $C^{\mathrm{OP}}_{\mathrm{M}}$, is expressed by

$$C^{\mathrm{OP}}_{\mathrm{M}} = \sum_{y\in\mathcal{Y}} p(y) \sum_{t\in\mathcal{T}}\sum_{n\in\mathcal{N}_{\mathrm{DC}}}\sum_{m\in\mathcal{M}} x_{m,n} \sum_{i_m\in\mathcal{I}_m} \{x_{i_m,n} \rho_{m,n}(t,y) E_{i_m,n}(t,y)\}. \tag{7}$$

### *B. Environmental Objective*

The second objective of the planning problem is to minimize the harmful GHG emissions by inserting EVs in the remote community as a substitute to the conventional fossil-fueled vehicles. The total emission $H^{\mathrm{T}}$ can be expressed as

$$H_{\mathrm{T}} = H_{\mathrm{D}} - H_{\mathrm{M}}, \tag{8}$$

where $H_{\mathrm{D}}$ denotes the total emissions due to the allocated dispatchable generators and $H_{\mathrm{M}}$ indicates the total emission reduction due to replacing conventional fossil fueled vehicles by EVs. The DG emissions are given by

$$H_{\mathrm{D}} = \sum_{y\in\mathcal{Y}} p(y) \sum_{t\in\mathcal{T}}\sum_{n\in\mathcal{N}_{\mathrm{AC}}}\sum_{d\in\mathcal{D}_1} x_{d,n} \mu_d P_{d,n}(t,y). \tag{9}$$

The total reduction in emissions due to the allocation of EV charging stations is given by

$$H_{\mathrm{M}} = \sum_{y\in\mathcal{Y}} p(y) \sum_{t\in\mathcal{T}}\sum_{n\in\mathcal{N}_{\mathrm{DC}}}\sum_{m\in\mathcal{M}} x_{m,n} \sum_{i_m\in\mathcal{I}_m} \{x_{i_m,n}\nu D E_{i_m,n}(t,y)\}. \tag{10}$$

### C. Technical Constraints

For every $n, t, y$, the power flow constraints at the AC buses $n, n' \in \mathcal{N}_{\text{AC}}$ are given by

$$\begin{aligned} P_n(t,y) &= \sum_{n' \in \mathcal{N}_{\text{AC}}} V_n(t,y) V_{n'}(t,y) Y_{n,n'} \cos(\theta_{n,n'} + \\ &\quad \delta_{n'}(t,y) - \delta_n(t,y)), \\ Q_n(t,y) &= \sum_{n' \in \mathcal{N}_{\text{AC}}} V_n(t,y) V_{n'}(t,y) Y_{n,n'} \sin(\theta_{n,n'} + \\ &\quad \delta_{n'}(t,y) - \delta_n(t,y)). \end{aligned} \tag{11}$$

On the other hand, the power flow constraints at the DC buses $n, n' \in \mathcal{N}_{\text{DC}}$ for every $n, t, y$ are given by

$$P_n(t,y) = \sum_{n' \in \mathcal{N}_{\text{DC}}} V_n(t,y) V_{n'}(t,y) G_{n,n'}. \tag{12}$$

The net injected active and reactive powers defined in (11) and (12) are given by

$$\begin{aligned} P_n(t,y) &= \sum_{d \in \mathcal{D}} x_{d,n} P_{d,n}(t,y) + \sum_{k \in \mathcal{K}} \gamma P_{k,n}(t,y) - \\ &\quad \sum_{m \in \mathcal{M}} x_{m,n} \sum_{i_m \in \mathcal{I}_m} x_{i_m,n} P_{i_m,n}(t,y) - P_{\text{L},n}(t,y), \\ Q_n(t,y) &= \sum_{d \in \mathcal{D}_1} x_{d,n} Q_{d,n}(t,y) + \sum_{k \in \mathcal{K}} \gamma Q_{k,n}(t,y) - \\ &\quad Q_{\text{L},n}(t,y), \end{aligned} \tag{13}$$

where $\gamma = 1$ to reflect an injected power at interlinking converter $k$ for $n \in \mathcal{N}_{\text{AC}}$ and $\gamma = -1$ to reflect a consumed power at interlinking converter $k$ for $n \in \mathcal{N}_{\text{DC}}$.

Furthermore, in (11) and (12), the voltage $V_n(t,y)$ should be within its upper and lower limits for every bus $n \in \mathcal{N}$, i.e.,

$$V^{\min} \leq V_n(t,y) \leq V^{\max}. \tag{14}$$

The following constraints hold for the AC/DC interlinking converters for every $t, y$

$$\begin{aligned} &P_{k,n}^2(t,y) + Q_{k,n}^2(t,y) \leq S_{k,n}^{\max\,2}, \quad \forall n \in \mathcal{N} \\ &Q_n(t,y) = 0, \quad \forall n \in \mathcal{N}_{\text{DC}}. \end{aligned} \tag{15}$$

For dispatchable generators, the generated active and reactive powers satisfy the following constraint

$$P_{d,n}^2(t,y) + Q_{d,n}^2(t,y) \leq S_{d,n}^{\max\,2}, \quad \forall d \in \mathcal{D}_1, n \in \mathcal{N}_{\text{AC}}, t \in \mathcal{T}. \tag{16}$$

In addition, the droop control enforces the following constraints for every $d \in \mathcal{D}_1, n \in \mathcal{N}_{\text{AC}}, t \in \mathcal{T}, y \in \mathcal{Y}$

$$\begin{aligned} P_{d,n}(t,y) &= (\alpha_{d,n}(t,y))^{-1} (\hat{\omega}_{d,n}(t,y) - \omega(t,y)), \\ Q_{d,n}(t,y) &= (\beta_{d,n}(t,y))^{-1} (\hat{V}_{d,n}(t,y) - V_n(t,y)). \end{aligned} \tag{17}$$

Moreover, the operation frequency within the microgrid satisfies the upper and lower limits, i.e., for all $n \in \mathcal{N}_{\text{AC}}, t \in \mathcal{T}, y \in \mathcal{Y}$

$$\omega^{\min} \leq \omega(t,y) \leq \omega^{\max}. \tag{18}$$

For every PV unit $d \in \mathcal{D}_2$, the generated active power satisfies the following constraint

$$P_{d,n}(t,y) \leq P_{d,n}^{\max} P_{\text{PV}}(t,y), \quad \forall n \in \mathcal{N}_{\text{DC}}, t \in \mathcal{T}, y \in \mathcal{Y}. \tag{19}$$

The consumed power by the EVs connected to charger $i_m$ in station $m$ allocated at bus $n$ can be described by

$$\begin{aligned} P_{i_m,n}(t,y) &= \sum_{m \in \mathcal{M}} \sum_{i_m \in \mathcal{I}_m} \frac{1}{\eta} z_{i_m,n}(t,y) P_{i_m,n}^{\text{CH}}(t,y), \\ &\quad \forall n \in \mathcal{N}_{\text{DC}}, t \in \mathcal{T}, y \in \mathcal{Y}, \end{aligned} \tag{20}$$

The charger power transfer limit $P_{i_m,n}^{\text{CH}}(t,y)$ can be expressed as

$$P_{i_m,n}^{\text{CH}}(t,y) = f(B_{i_m,n}^{\text{FN}}(t,y)), \tag{21}$$

where $f(\cdot)$ is a function that describes the characteristics of the EV battery connected to charger $i_m$ in station $m$ that is allocated at bus $n \in \mathcal{N}_{\text{DC}}$. The energy delivered to the EVs due to charger $i_m$ in station $m$ on bus $n \in \mathcal{N}_{\text{DC}}$ is given by

$$E_{i_m,n}(t,y) = E_{i_m,n}^{\max} \{B_{i_m,n}^{\text{FN}}(t,y) - B_{i_m,n}^{\text{INT}}(t,y)\}. \tag{22}$$

The final battery SOC for the EV connected at charger $i_m$ in station $m$ on bus $n \in \mathcal{N}_{\text{DC}}$ is limited by the desirable SOC, i.e.,

$$B_{i_m,n}^{\text{FN}}(t,y) \leq B_{i_m,n}^{\text{DES}}(t,y). \tag{23}$$

The update of the SOC from one time period to the next one can be described as follows

$$B_{i_m,n}^{\text{FN}}(t+1,y) = B_{i_m,n}^{\text{FN}}(t,y) + \frac{z_{i_m,n}(t,y) P_{i_m,n}^{\text{CH}}(t,y)}{E_{i_m,n}^{\max}}. \tag{24}$$

To ensure a sustainable power flow in the remote microgrid, the sizes of the DG units should present a sufficient margin as a reserve in case of failures and to serve the load growth, i.e.,

$$\sum_{n \in \mathcal{N}} \sum_{d \in \mathcal{D}} P_{d,n}^{\max} \geq \delta \sum_{n \in \mathcal{N}} \{P_{\text{L},n}^{\max} + \sum_{m \in \mathcal{M}} \sum_{i_m \in \mathcal{I}_m} P_{i_m,n}(t,y)\}, \tag{25}$$

with $\delta > 1$. Moreover, the dispatchable DGs should be able to serve the loads in the remote microgrid when the PV units are partially or totally unavailable, and hence,

$$\sum_{n \in \mathcal{N}} \sum_{d \in \mathcal{D}_1} P_{d,n}^{\max} \geq \kappa \sum_{n \in \mathcal{N}} \{P_{\text{L},n}^{\max} + \sum_{m \in \mathcal{M}} \sum_{i_m \in \mathcal{I}_m} P_{i_m,n}(t,y)\}, \tag{26}$$

where $\kappa < 1$.

### D. Optimal Planning Problem

Define the following allocation and sizing decision variables: $\mathbf{X} = \{x_{d,n}, x_{m,n}, x_{i_m,n} \ \forall n \in \mathcal{N}, d \in \mathcal{D}, m \in \mathcal{M}, i_m \in \mathcal{I}_m\}$, $\mathbf{P}^{\max} = \{P_{d,n}^{\max}, P_{i_m,n}^{\max} n \in \mathcal{N}, d \in \mathcal{D}, m \in \mathcal{M}, i_m \in \mathcal{I}_m\}$, $\mathbf{S}^{\max} = \{S_{d,n}^{\max} \ \forall n \in \mathcal{N}, d \in \mathcal{D}\}$. Furthermore, the operational decision variables are defined as: $\mathbf{Z} = \{z_{i_m,n}(t,y) \ \forall n \in \mathcal{N}_{\text{DC}}, m \in \mathcal{M}, i_m \in \mathcal{I}_m, t \in \mathcal{T}, y \in \mathcal{Y}\}$, $\mathbf{P} = \{P_n(t,y), P_{d,n}(t,y), P_{i_m,n}(t,y), P_{k,n}(t,y) \ \forall n \in \mathcal{N}, d \in \mathcal{D}, m \in \mathcal{M}, i_m \in \mathcal{I}_m, k \in \mathcal{K}, t \in \mathcal{T}, y \in \mathcal{Y}\}$, $\mathbf{Q} = \{Q_n(t,y), Q_{d,n}(t,y), Q_{k,n}(t,y) \ \forall n \in \mathcal{N}, d \in \mathcal{D}_1, k \in \mathcal{K}, t \in \mathcal{T}, y \in \mathcal{Y}\}$, and the droop control variables are $\mathbf{\Psi} = \{\alpha_{d,n}(t,y), \beta_{d,n}(t,y), \hat{\omega}_{d,n}(t,y), \hat{V}_{d,n}(t,y) \ \forall n \in \mathcal{N}, d \in \mathcal{D}_1, t \in \mathcal{T}, y \in \mathcal{Y}\}$. The multi-objective joint planning problem can be expressed as

$$\begin{aligned} \min_{\mathbf{X}, \mathbf{P}^{\max}, \mathbf{S}^{\max}, \mathbf{Z}, \mathbf{P}, \mathbf{Q}, \mathbf{\Psi}} \quad & (C_{\text{T}}, H_{\text{T}}) \\ \text{s.t.} \quad & (11) - (26), \\ & \mathbf{X}, \mathbf{Z} \in \{0,1\}, \end{aligned} \tag{27}$$

with $C_{\text{T}}$ and $H_{\text{T}}$ described by (1) - (7) and (8) - (10), respectively. The optimization in (27) jointly allocates and sizes DG units and EV charging stations, through the decision variables $\mathbf{X}, \mathbf{P}^{\max}$, and $\mathbf{S}^{\max}$, in order to minimize the total cost and emissions in the remote microgrid. The optimization in (27) satisfies the operational technical constraints on the decision variables $\mathbf{Z}, \mathbf{P}, \mathbf{Q}$, and $\mathbf{\Psi}$. The joint planning problem presents two conflicting objectives and a set of binary decision variables ($\mathbf{X}$ and $\mathbf{Z}$) and continuous decision variables ($\mathbf{P}^{\max}, \mathbf{S}^{\max}, \mathbf{P}, \mathbf{Q}$, and $\mathbf{\Psi}$). Moreover, many of the constraints in (11)-(26) are non-linear. As a result, (27) represents a multi-objective MINLP, which is NP-hard and incurs high computational complexity. In order to efficiently solve the joint planning problem (27), a two-stage planning algorithm is presented in the next section.

## IV. Joint Planning Algorithm

The proposed joint planning algorithm solves (27) iteratively via outer and inner sub-problems. The outer sub-problem determines the allocation and sizing decisions $\mathbf{X}, \mathbf{P}^{\max}$, and $\mathbf{S}^{\max}$, and hence, calculates the annualized CAPEX. The inner sub-problem then tackles the operational aspects of (27) by specifying $\mathbf{Z}, \mathbf{P}, \mathbf{Q}$, and $\mathbf{\Psi}$, and hence, determining the levelized OPEX and the corresponding emissions. Further details about the joint planning algorithm is given in the next subsections.

### A. Allocation and Sizing Sub-problem

The first sub-problem aims to jointly allocate and size the DGs and EV charging stations in the remote microgrid. The proposed solution should satisfy the load growth and availability constraints in (25) and (26), respectively. In order to efficiently solve such an allocation and sizing problem especially in a large microgrid, heuristic optimization techniques can be adopted. In this work, the NSGA-II is employed as it offers a reduced computational complexity and faster convergence time compared with other heuristic techniques [19].

A set of candidate buses are selected for the allocation of dispatchable generators, $\mathcal{N}_{\text{D}_1}$, PV units, $\mathcal{N}_{\text{D}_2}$, and EV charging stations, $\mathcal{N}_{\text{M}}$, according to techno-economical studies. The NSGA-II is a population-based algorithm. Each population consists of a set of individuals (chromosomes). Each individual adopts the following structure: the first group of elements, $|\mathcal{N}_{\text{D}_1}| \times |\mathcal{D}_1|$, specifies the allocation and sizing of dispatchable generators, the next group, $|\mathcal{N}_{\text{D}_2}| \times |\mathcal{D}_2|$, specifies the allocation and sizing of the PV units, and the last group, $2 \times |\mathcal{N}_{\text{M}}| \times |\mathcal{M}|$, specifies the allocation and sizing of the EV charging stations, where $|\mathcal{A}|$ denotes the cardinality of set $\mathcal{A}$. For the dispatchable generators, each group of $|\mathcal{N}_{\text{D}_1}|$ elements specifies the allocation and sizing decision variables for a given technology in $\mathcal{D}_1$. Consider a given group of $|\mathcal{N}_{\text{D}_1}|$ elements. If an element value equals 0, then the corresponding technology in $\mathcal{D}_1$ shall not be allocated in the the candidate bus represented by that element. Otherwise, the value assigned to that element represents the capacity $S_{d,n}$ of the allocated generator from the corresponding technology on the candidate bus. Similarly, the allocation and sizing of the PV units follows the same approach. For the allocation and sizing of the EV charging stations, consider a given group of $|\mathcal{N}_{\text{M}}|$ elements. If an element value equals 0, then no charging station is allocated on the candidate bus represented by that element. Otherwise, the value assigned to that element represent the number of chargers installed in the charging station allocated on that candidate bus, and the corresponding element on the next $|\mathcal{N}_{\text{M}}|$ group specifies the capacity $P^{\max}_{i_m,n}$ per installed charger. The structure of the individual is illustrated in Figure 1.

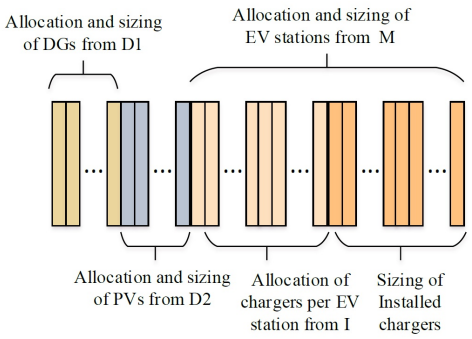


Fig. 1. Illustration of the chromosome structure.

The outer sub-problem is solved via the following steps:

1) A population $\mathcal{G}_g$ of size $|\mathcal{G}_g|$ individuals (with $g = 0$ initially) is randomly generated such that the constraints (25) and (26) are satisfied.
2) The annualized CAPEX $C_{\text{CT}}$ is calculated for the individuals in $\mathcal{G}_g$.
3) The inner sub-problem is called in order to check the operational feasibility of the allocation and sizing decisions and to calculate the expected levelized OPEX $C^{\text{OP}}$ and the expected total emissions $H_{\text{T}}$, as will be explained in Section IV.B. If the allocation and sizing decision vector of a given individual is infeasible, a large penalty value is assigned as the expected levelized OPEX and emissions, e.g., $C^{\text{OP}} = H_{\text{T}} = 10^{20}$.
4) Two Fitness values are now associated with each individual in $\mathcal{G}_g$, namely, $F_1^{\mathcal{G}_g} = C_{\text{CT}} + C^{\text{OP}}$ and $F_2^{\mathcal{G}_g} = H_{\text{T}}$.
5) An off-spring population $\tilde{\mathcal{G}}_g$ is generated from $\mathcal{G}_g$ via tournament selection, recombination, and mutation. The annualized CAPEX $C_{\text{CT}}$ is calculated for the individuals in $\tilde{\mathcal{G}}_g$. The inner sub-problem is also called to check the feasibility of the individuals in $\tilde{\mathcal{G}}_g$ and to calculate the expected levelized OPEX $C^{\text{OP}}$ and the expected total emissions $H_{\text{T}}$. Two Fitness values are also associated with each individual in $\tilde{\mathcal{G}}_g$, namely, $F_1^{\tilde{\mathcal{G}}_g} = C_{\text{CT}} + C^{\text{OP}}$ and $F_2^{\tilde{\mathcal{G}}_g} = H_{\text{T}}$.
6) The populations $\mathcal{G}_g$ and $\tilde{\mathcal{G}}_g$ are recombined and their individuals are ranked according to their non-dominance. Specifically, an individual $\vec{a}_1$ has a rank $R_1$ if it is not dominated by any other individual in terms of the two fitness values $F_1$ and $F_2$, i.e., there is no other individual $\vec{a}$ where $F_1(\vec{a}) < F_1(\vec{a}_1)$ and $F_2(\vec{a}) < F_2(\vec{a}_1)$. An individual with rank $R_2$ is dominated by only one individual, and so on.

7) A new population is now formed for the next iteration using the non-dominated sorting of the individuals of the combined generations $\mathcal{G}_g$ and $\tilde{\mathcal{G}}_g$. Let $g \leftarrow g+1$. The new population $\mathcal{G}_g$ should have the same size as the original population. This is achieved by considering all individuals with rank $R_1$, then rank $R_2$, and so on. In case that the individuals of a given rank $R_r$ result in a larger population size for the new $\mathcal{G}_g$ when added to the individuals of higher ranks, only a subset of individuals with rank $R_r$ is considered such that the correct size of $\mathcal{G}_g$ is obtained. In order to specify which individuals with rank $R_r$ to be considered in $\mathcal{G}_{g+1}$, crowd distance sorting is applied to the individuals with rank $R_r$. Crowd distance sorting within individuals of $R_r$ results in a more diverse solution in the Pareto frontier by selecting individuals with less density. The crowd distance is calculated first for each fitness function of each individual by calculating the difference between the two fitness values to the right and left of that individual. Then, the the overall crowd distance of that individual is calculated by summing the crowd distance calculated for the two fitness functions. The individuals within rank $R_r$ are then sorted in descending order of their crowd distance and the top most individuals are selected to complete the new population $\mathcal{G}_g$.
8) If the total number of generations (iterations) is not met, go to step 2, else go to the next step.
9) The Pareto front is specified by the set of individuals with rank $R_1$. In order to achieve an acceptable trade-off between the two conflicting objectives, a compromise solution is calculated as explained in Section IV.C.

### *B. Operation Sub-problem*

The inner sub-problem checks the operational feasibility of the candidate solution obtained by the outer sub-problem, and if feasible, the levelized OPEX and the corresponding emissions are determined. To reduce the computational complexity, the inner sub-problem first solves the following relaxed OPEX minimization sub-problem for a given scenario $y \in \mathcal{Y}$

$$\begin{aligned} \min_{\mathbf{Z},\mathbf{P},\mathbf{Q},\mathbf{\Psi}} \quad & C_{\text{OT}} \\ \text{s.t.} \quad & (11)-(24), 0 \leq \mathbf{Z} \leq 1. \end{aligned} \tag{28}$$

As shown in (28), the binary decision variable $\mathbf{Z}$ is relaxed to be a continuous variable. Hence, (28) is simplified to a non-linear program (NLP). In order to find a global solution for (28), we first remove the trigonometric functions in the power flow constraints in (11) using Taylor expansion. The modified power flow constraints can be expressed as follows

$$\begin{aligned} P_n(t,y) = & \sum_{n' \in \mathcal{N}_{\text{AC}}} V_n(t,y)V_{n'}(t,y)\{\Re(Y_{n,n'})(1- \\ & \frac{\Lambda^2_{n,n'}(t,y)}{2}) - \Im(Y_{n,n'})(\Lambda_{n,n'}(t,y) - \frac{\Lambda^3_{n,n'}(t,y)}{3})\}, \\ Q_n(t,y) = & \sum_{n' \in \mathcal{N}_{\text{AC}}} V_n(t,y)V_{n'}(t,y)\{\Im(Y_{n,n'})(1- \\ & \frac{\Lambda^2_{n,n'}(t,y)}{2}) - \Re(Y_{n,n'})(\Lambda_{n,n'}(t,y) - \frac{\Lambda^3_{n,n'}(t,y)}{3})\}, \end{aligned} \tag{29}$$

where $\Re(Y_{n,n'}) = Y_{n,n'}\cos(\theta_{n,n'})$, $\Im(Y_{n,n'}) = Y_{n,n'}\sin(\theta_{n,n'})$, and $\Lambda_{n,n'}(t,y) = \delta_{n'}(t,y) - \delta_n(t,y)$. Now, the global solver BARON can be used to solve the operation sub-problem by solving (28) while replacing (11) by (29). Upon calculating the expected levelized OPEX, i.e., say $C_{\text{OT}} = \Sigma$, the emission minimization sub-problem is written as follows

$$\begin{aligned} \min_{\mathbf{Z},\mathbf{P},\mathbf{Q},\mathbf{\Psi}} \quad & H_{\text{T}} \\ \text{s.t.} \quad & (12)-(24),(29), C_{\text{OT}} = \Sigma \\ & 0 \leq \mathbf{Z} \leq 1. \end{aligned} \tag{30}$$

The minimization (30) is also solved using BARON to specify the expected total emissions for the scenario $y \in \mathcal{Y}$. It should be noted that the minimization problems (28) and (30) are solved sequentially for each scenario $y \in \mathcal{Y}$, and the final expected levelized OPEX and total emissions are calculated by summing the obtained weighted solutions (with weight $p(y)$) over all scenarios.

The inner sub-problem is solved via the following steps:

1) Do the following for each individual in $\mathcal{G}_g$:
2) Do the following for each scenario $y \in \mathcal{Y}$:
3) Solve the operational minimization sub-problem (28) while considering the modified power flow equations (29).
4) If the operational minimization sub-problem is infeasible, set $C_{\text{OT}}$ and $H_{\text{T}}$ to a high penalty value, e.g., $10^{20}$. Otherwise, solve the emission minimization sub-problem (31).
5) Go to step 2 if more scenarios still exist in $\mathcal{Y}$, otherwise, calculate the expected levelized OPEX for that individual by summing a weighted version of the calculated $C_{\text{OT}}$ overall scenarios. The same is also done to calculate the expected total emissions for that individual.
6) Go to step 1 if more individuals still exist in $\mathcal{G}_g$, otherwise, stop.

### *C. Compromise Solution*

Any point on the Pareto frontier can be chosen as an optimal solution for the joint planning problem according to the preference of the microgrid operator. However, it is widely accepted to select a compromise solution on the Pareto frontier that minimizes the distance between the Pareto frontier and an ideal solution that is referred to as the utopia point [19]. This ideal solution minimizes both the total cost and the total GHG emissions, which is impossible to achieve in practice as both objectives are conflicting. Hence, the utopia point lies outside the feasible region. The normalized distance between the utopia point and a point $j$ on the Pareto frontier is given by

$$\Upsilon_j = \sqrt{\sum_{l=1}^{2} \frac{(F_l(\sigma_j) - F_l(\sigma_l))^2}{F_l^2(\sigma_l))}}, \tag{31}$$

where $F_1(\cdot)$ and $F_2(\cdot)$ denote the two conflicting objectives, namely, the total cost and total emissions, respectively, $\sigma_j$ captures the decision variables related to point $j$ on the Pareto frontier, and $\sigma_l$ represents the decision variables that

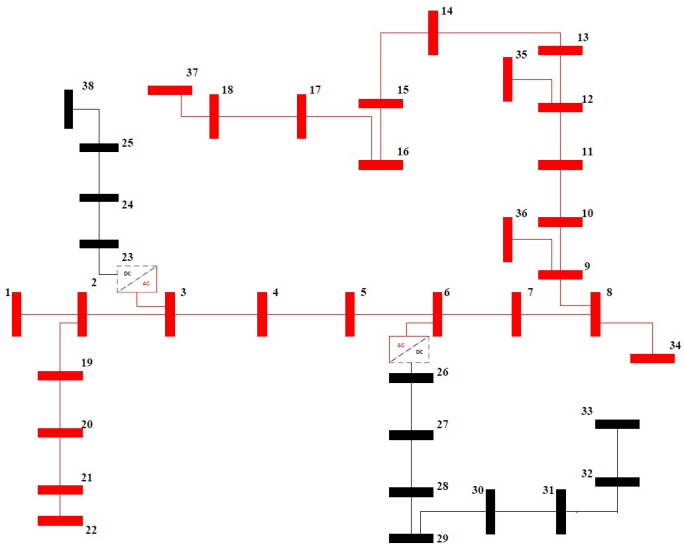


Fig. 2. Schematic of the hybrid AC/DC 38-bus test system under consideration.

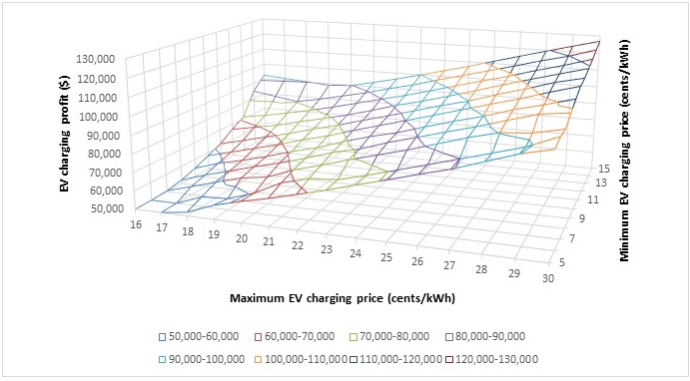


Fig. 3. Impact of EV charging price on the joint planning.

minimizes the objective $F_l(\cdot)$ for $l = 1, 2$. The compromise point is the point on the Pareto frontier that results in the minimum $\Upsilon_j$ among all the points on the frontier. In this work, the compromise point is selected as the solution to the joint planning problem in (27).

## V. Simulation Results and Discussions

The proposed joint planning algorithm is tested on a 38-bus radial distribution system, as shown in Figure 2. Two AC/DC interlinking converters are installed between buses 3 and 23 and between buses 6 and 26 in the microgrid to connect the AC and DC sections. The remote microgrid has total regular active and reactive power demands of 3.715 MW and 2.3 Mvar, respectively. The upper and lower voltage and frequency limits are $V^{\min} = 0.9$, $V^{\max} = 1.1$, $\omega^{\min} = 0.99$, and $\omega^{\max} = 1.01$. Natural gas DG units is chosen for the dispatchable generators set $\mathcal{D}_1$, which presents a base supply for the remote microgrid. The CAPEX for the natural gas DG units is $1,104,000$ [20]. The fuel escalation factor is $3\%$. The candidate buses for the allocation of the dispatchable DG units are $\mathcal{N}_{\mathrm{D}_1} = \{1, 4, 10, 22, 34, 37\}$. The CAPEX of the PV unit in $\mathcal{D}_2$ is $2,500,000$ \$. The candidate buses for the allocation of the PV units are $\mathcal{N}_{\mathrm{D}_2} = \{24, 25, 29, 32\}$. The EV charging stations in $\mathcal{C}$ has a minimum chargers of 5 and maximum chargers of 200, and each charger has a capacity of 7 kW and a CAPEX of 4000 \$. The candidate buses for the allocation of the EV charging stations are $\mathcal{N}_{\mathrm{M}} = \{23, 27, 33, 38\}$. The interest rate is $10\%$. Let $\gamma = 1.2$ and $\kappa = 70\%$.

First, we investigate the impact of the EV charging price on the EV charging profit. Given the linear charging price model described in Section II, a large price would discourage customers from using EVs, which in turn would have a negative effect on the environment due to the resulting emissions. In this case study, we consider only a single objective of minimizing the total cost in the microgrid. Learning the appropriate EV charging price parameters ($\rho^{\max}$ and $\rho^{\min}$) from this case study, we then test the multi-objective joint planning algorithm and specify the compromise solution that balances both the total cost and the carbon dioxide emissions. In this case study, the fuel price for the dispatchable generators is fixed at 35 \$/MWh for DDG. The maximum and minimum EV charging prices ($\rho^{\max}$ and $\rho^{\min}$) are varried as shown in Figure 3. The EV charging profit shown in Figure 3 is the levelized revenue after subtracting the CAPEX of the EV chargers. As shown in Figure 3, the profit almost increases with a rate or $4,110$ \$ per each 1 cent/kWh increase in the maximum EV charging price. Increasing the maximum price while fixing the minimum EV charging price lead to higher EV required charging energy for same offered price, as shown in Figure 3. On the other hand, increasing the minimum EV charging price while keeping the same maximum energy price have the same effect on the revenue, except that the increase in the revenue is less, which is about $3,380$ \$ per 1 cent/kWh increase.

From the aforementioned study, feasible ranges for the fuel price of the dispatchable generators and the maximum and minimum EV charging prices are specified. These values can be used in the study that presents a multi-objective joint planning with focus on two objectives: total system annulaized cost and annual emissions. These two objectives are usually contradicting as the low cost DG units have considerable contribution to the GHG emissions while clean renewable resources such as PV-based DG units have high CAPEX. In addition to DG units, the EV charging effect on reducing the GHG emissions is considered. Every kWh of EV charging replaces an amount of gasoline that have negative impact on the environment. Thus, the EV charging effect on emissions is assumed always to be a reduction. As shown in Figure 4, the result of the Pareto front shows possible solutions for the investor in terms of costs and corresponding emissions. Two extreme solutions can be noticed in the figure, namely, minimum emissions solution A and minimum cost solution B. The details of each solution are as follow. Solution A is characterized by total annual emissions of $5,034,808$ kg $CO_2$ and total annual cost of $1,869,558$ \$. The allocated DG capacities are 5 MW and 1.67 MW for dispatchable DGs and PV-based DGs, respectively. This is the maximum allowable allocated capacity of dispatchable DGs and PV-

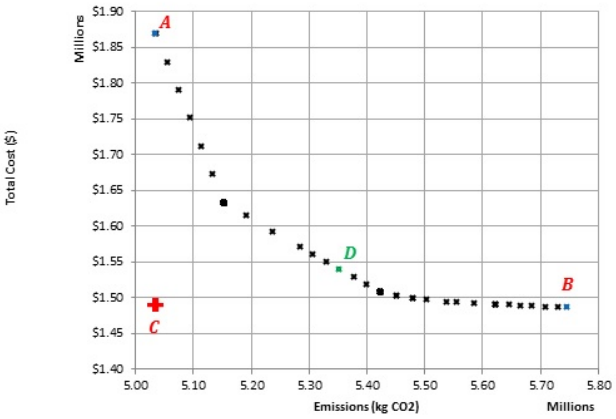


Fig. 4. Pareto front for the joint planning problem.

based DGs as the PV-based DGs are allowed only up to 30 % of the dispatchable DGs' capacity. Such maximum allowable capacities are deployed in order to be able to support 200 allocated chargers in the remote microgrid, which represents the maximum limit. The emissions from the dispatchable generators are $6,271,437$ kg $CO_2$, while the reduction due to EV charging is $1,236,629$ kg $CO_2$, which is equivalent to $19.7$ % reduction in the dispatchable DG emissions. On the other hand, solution B is characterized by a minimum cost of $1,486,793$ \$ and annual emissions of $5,746,948$ kg $CO_2$. Hence, the emissions are increased by $14.14$ % and the costs are reduced by $20.5$ % compared with solution A. Solution B allocates $3.467$ MW of dispatchable DGs, zero PV-based DGs, and $85$ EV chargers. The utopia point, which represents the minimum system costs and the minimum system emissions, is defined as solution C, which lies outside the feasible region, as shown in Fig. 4. The costs and emissions for this ideal scenario are $1,486,793$ and $5,034,808$ kg $CO_2$, respectively. The normalized distance criteria presented in (31) is used to find a possible compromising solution for the investors, which is defined to be point D as shown in Figure 4. Solution D is characterized by emissions of $5,353,321$ kg $CO_2$ and cost of $1,539,557$ \$. Solution D suggests allocating $3.57$ MW of dispatchable DGs, $0.30$ MW of PV-based DGs, and 200 EV chargers, which is the maximum limit for EV chargers. This compromising solution has only $6.3$ % more emissions than solution A and $3.5$ % more costs than solution B.

## VI. Conclusions

A joint planning algorithm is presented in this paper to allocate both DG units and EV charging stations in remote hybrid microgrids. The objective of the planning algorithm is to minimize the total costs including both CAPEX and OPEX while promoting an eco-friendly community by minimizing the associated GHG emissions as well. The joint planning solution satisfies the microgrid technical constraints for power flow, sustainability, and reliability. The planning algorithm results in a Pareto frontier that offers a set of optimal solutions presenting a trade-off between the economical and environmental objectives. Furthermore, the planning algorithm suggests a compromise solution that presents an attractive balance between the two conflicting objectives.

## References


[1] S. Hadley and A. Tsvetkova, "Potential impacts of plug-in hybrid electric vehicles on regional power generation," *Electricity Journal*, vol. 22, no. 10, pp. 56-68, Dec. 2009.

[2] S. Letendre and R. Watts, "Effects of plug-in hybrid electric vehicles on the Vermont electric transmission system," *Proceedings of Transportation Research Board Annual Meeting*, pp. 11-15, 2009.

[3] M. F. Shaaban, M. Ismail, E. El-Saadany and W. Zhuang, "Real-time PEV charging/discharging coordination in smart distribution systems," *IEEE Transactions on Smart Grid*, vol. 5, no. 4, pp. 1797-1807, July 2014.

[4] I. S. Bayram, M. Ismail, M. Abdallah, K. Qaraqe, and E. Serpedin, "A pricing-based load shifting framework for EV fast charging stations," *Proceedings of IEEE International Conference on Smart Grid Communications (SmartGridComm)*, pp. 680-685, 2014.

[5] M. Wang, M. Ismail, X. Shen, E. Serpedin, and K. Qaraqe, "Spatial and temporal online charging/discharging coordination of mobile PEVs," *IEEE Wireless Communications*, vol. 22, no. 1, pp. 112-121, Feb. 2015.

[6] M. Wang, M. Ismail, R. Zhang, X. Shen, E. Serpedin, and K. Qaraqe, "A semi-distributed V2V fast charging strategy based on price control," *Proceedings of IEEE Global Communications Conference (GLOBECOM)*, pp. 4550-4555, 2014.

[7] M. Wang, M. Ismail, R. Zhang, X. Shen, E. Serpedin, and K. Qaraqe, "Spatio-temporal coordinated V2V energy swapping strategy for mobile PEVs," *IEEE Transactions on Smart Grid*, vol. 9, no. 3, pp. 1566-1579, May 2018.

[8] B. Sun, Z. Huang, X. Tan and D. Tsang, "Optimal scheduling for electric vehicle charging with discrete charging levels in distribution grid," *IEEE Transactions on Smart Grid*, vol. 9, no. 2, pp. 624-634, March 2018.

[9] K. Kaur, N. Kumar and M. Singh, "Coordinated power control of electric vehicles for grid frequency support: MILP-based hierarchical control design," *IEEE Transactions on Smart Grid*, Early Access.

[10] Y. Kim, J. Kwak and S. Chong, "Dynamic pricing, scheduling, and energy management for profit maximization in PHEV charging stations," *IEEE Transactions on Vehicular Technology*, vol. 66, no. 2, pp. 1011-1026, Feb. 2017.

[11] L. Yao, W. H. Lim and T. S. Tsai, "A Real-Time Charging Scheme for Demand Response in Electric Vehicle Parking Station," *IEEE Transactions on Smart Grid*, vol. 8, no. 1, pp. 52-62, Jan. 2017.

[12] J. Wang, G. R. Bharati, S. Paudyal, O. Ceylan, B. P. Bhattarai and K. S. Myers, "Coordinated electric vehicle charging with reactive power support to distribution grids," *IEEE Transactions on Industrial Informatics*, Early Access.

[13] M. Ismail, I. S. Bayram, M. Abdallah, E. Serpedin, and K. Qaraqe, "Optimal planning of fast PEV charging facilities," *Proceedings of First Workshop on Smart Grid and Renewable Energy (SGRE)*, pp. 1-6, 2015.

[14] K. Chaudhari, A. Ukil, K. Kumar, U. Manandhar and S. Kollimalla, "Hybrid optimization for economic deployment of ESS in PV-integrated EV charging stations," *IEEE Transactions on Industrial Informatics*, vol. 14, no. 1, pp. 106-116, Jan. 2018.

[15] M. F. Shaaban and E. F. El-Saadany, "Accommodating high penetrations of PEVs and renewable DG considering uncertainties in distribution systems," *IEEE Transactions on Power Systems*, vol. 29, no. 1, pp. 259-270, Jan. 2014.

[16] A. Awad, M. F. Shaaban, T. EL-Fouly, E. El-Saadany and M. Salama, "Optimal resource allocation and charging prices for benefit maximization in smart PEV-parking lots," *IEEE Transactions on Sustainable Energy*, vol. 8, no. 3, pp. 906-915, July 2017.

[17] H. Simorgh, H. Mojarrad, H. Razmi and G. Gharehpetian, "Cost-based optimal siting and sizing of electric vehicle charging stations considering demand response programmes," *IET Generation, Transmission & Distribution*, vol. 12, no. 8, pp. 1712-1720, April 2018.

[18] Gilbert M. Masters, "Renewable and efficient electric power systems," *John Wiley & Sons*, 2013.

[19] K. Deb, A. Pratap, S. Agarwal and T. Meyarivan, "A fast and elitist multiobjective genetic algorithm: NSGA-II," *IEEE Transactions on Evolutionary Computation*, vol. 6, pp. 182-197, 2002.

[20] U.S. Department of Energy, "Capital cost estimates for utility scale electricity generating plant," Nov. 2016.